*Progress In Electromagnetics Research M, Vol. 87, 103–113, 2019*

# Compact Dual-Band Circularly Polarized Patch Antenna with Wide 3-dB Axial Ratio Beamwidth for BeiDou Applications

**Hongmei Liu*, Chenhui Xun, Shaojun Fang, and Zhongbao Wang**

**Abstract**—A dual-band circularly polarized (CP) patch antenna with wide 3-dB axial ratio beamwidth (ARBW) is presented for BeiDou Navigation System (BDS). Simple stacked circular patches are used as the main radiations for achieving dual-band operation. To enhance the ARBW for the two operation bands, an annular metal strip loaded ground plane (AMSL-GP) is presented. Besides, edge resistors are inserted to the GP for further ARBW enhancement at the lower band. In realization, a compact single-input feed network based on a coupled-line trans-directional (CL-TRD) coupler is designed to provide two orthogonal modes at the two frequency bands simultaneously. Experimental results show that the bandwidth for 10-dB return loss is from 1.15 GHz to 1.65 GHz, which covers BDS B1 (1.561 GHz) and B2 (1.207 GHz). The 3-dB axial ratio (AR) bandwidths for the lower and upper bands are 9.6% and 7.1%, respectively. At 1.207 GHz, the antenna has 3-dB ARBWs of 185° and 187° in the $xoz$ and $yoz$ planes, respectively. And the values are 192° and 194° at 1.561 GHz.

## 1. INTRODUCTION

Global navigation satellite systems have been intensively used in many areas such as navigation, positioning, public safety, and surveillance. Compass Navigation Satellite System, officially named as BeiDou Navigation Satellite System (BDS), is expected to provide global positioning services in 2020. For high-accuracy positioning, circularly polarized (CP) antennas with right-hand circular polarization (RHCP) radiation, medium gain, wide axial-ratio beamwidth (ARBW), and compact size are required, wherein the size and ARBW are more critical than the gain and bandwidth to provide wide coverage and sufficient multi-path suppression [1]. For instance, a CP antenna usually needs to be developed with a 3-dB ARBW of more than 120° to ensure that wireless signal can be well received no matter whether the satellites are in low or high elevations [2, 3].

Generally speaking, a wide ARBW can be achieved by helix antennas [4, 5], modified turnstile antennas [6], and microstrip antennas [7–14]. Compared with helix and turnstile antennas, microstrip antennas are more preferred for the advantages of low-profile, light weight, and compact structure. However, 3-dB ARBWs of conventional CP microstrip antennas (CPMAs) are narrow. In the past, numerous methods were proposed to widen the 3-dB ARBW of CPMAs, such as adopting 3-D ground planes [7–9], loading additional radiation elements [10, 11], utilizing the aperture area of antennas [12–14], and spacing two pairs of parallel dipoles in a square contour [3]. However, the CP antennas using 3-D ground planes [7–9] and additional radiation elements [10, 11] suffer from high profile, and their complex in geometry may lead to difficulty in fabrication. The antenna in [3] showed unwanted bidirectional radiation patterns. In [12], a suspended structure with reduced effective permittivity was proposed for determining the radiating area, but the performance of the antenna was very sensitive to the error in installation of suspended height. In [13, 14], pin-loaded technique was utilized to present a wide 3 dB ARBW. However, the structures were not suitable for electrically small antennas, and the

*Received 5 September 2019, Accepted 19 November 2019, Scheduled 12 December 2019*
* Corresponding author: Hongmei Liu (lhm323@dlmu.edu.cn).
The authors are with the School of Information Science and Technology, Dalian Maritime University, Dalian, Liaoning 116026, China.

ARBWs became narrow when using finite ground. Besides, these technologies were mainly studied for single-band applications only.

Although many techniques have been reported to realize dual-band CP antennas, most of them are concentrated on bandwidth and size. In [15], two shorting probes in parallel were loaded on a dual-band GNSS antenna, which had a compact size of $0.25\lambda_g \times 0.25\lambda_g \times 0.072\lambda_g$. For further size reduction, a more compact dual-band CP antenna was proposed by using a meandered-line-shaped ring patch combined with a rectangular-ring patch [16]. For bandwidth enhancement, techniques such as aperture feeding [17] and broadband four-feed circuit [18] were presented. However, since the 3-dB ARBW was not considered [15–18], the reception of signals may be deteriorated when the satellites were in low or high elevations. To solve the problem, a dual-band CPMA with wide 3-dB ARBW was reported by extending the substrate beyond the ground plane [19]. However, the impedance and AR bandwidths were narrow. In [20, 21], cross dipoles combined with the cavity-backed reflectors were presented for enhanced 3-dB ARBW. However, high profile, complexity, and high cost were generated by the structure.

In this paper, a dual-band CPMA resonant at BDS B1 (1.561 GHz) and B2 (1.207 GHz) is presented with wide 3-dB ARBW. To enhance the ARBW, novel annular metal strip loaded ground plane (AMSL-GP) is presented. Besides, edge resistors are inserted to the GP for further ARBW enhancement at the lower band. Evolutions of the proposed AMSL-GP, as well as the inserted edge resistors, are introduced, and the parametric studies are investigated. For demonstration, a prototype fed by a compact single-input feed network is designed, fabricated, and measured. Comparisons are also presented between the design and some previous dual-band CP antennas.

## 2. ANTENNA STRUCTURE

Figure 1 depicts the structure of the proposed dual-band CPMA with wide 3-dB ARBW. It consists of three layers of substrates (top, middle, and bottom substrates), two radiating patches (upper and lower circular patches), the AMSL-GP and CL-TRD based feed network. A substrate F4B is used in the fabrication with a relative permittivity of 3, loss tangent of 0.003, and thickness of 1.5 mm. As shown in Figure 1(a), the radiation structure contains two concentric stacked patches: 1) a circular patch which contributes to the resonant mode of the upper frequency band is printed on the upper surface of the top substrate; 2) a circular patch printed on the upper surface of the bottom substrate contributes to the resonant mode of the lower frequency band. The radii of the upper and lower band radiation patches are $R_1$ and $R_2$, respectively. Each of the circular patches is fed by orthogonal modes via probes.

To improve the 3-dB ARBW at the two operation bands, the AMSL-GP with edge resistors is proposed and printed on the lower surface of the bottom substrate, as shown in Figure 1(b). It is formed by a circular ground patch with radius of $R_3$, an inner annular metal strip (AMS) with internal radius of $R_4$ and external radius of $R_5$, an outer AMS with internal radius of $R_6$ and external radius of $R_7$, and edge resistors with resistance of $R_L$. It is noted that the inner AMS is divided into 8 sections by identical air gaps with the length of $d_5$, while the outer AMS is divided into 4 sections by using identical chip resistors with the length of $d_6$. The inner AMS is used to improve the 3-dB ARBW of the upper band, and the outer AMS combined with the resistors is used for the lower band. Thus, the AMSL-GP can enhance the ARBW for dual-band operation.

To provide two orthogonal modes on the two patches, a single-input feed network capable of simultaneously operating at the upper and lower bands is proposed, as shown in Figure 1(c). It consists of two CL-TRD couplers, a 90° phase shifter, and a T-type power divider. The CL-TRD coupler, which is first introduced by Shie et al., can achieve tight coupling with weak coupled microstrip lines and allow decoupling the direct current patch between input and output ports [22]. Small size is also obtained compared with a branch-line coupler. In the design, a modified CL-TRD coupler [23] with improved power distribution and phase performance is applied to produce equal amplitude and consistent 90° phase shifts. To suppress the mutual coupling between the upper and lower radiation patches, a 90° phase shifter is connected to the lower band CL-TRD coupler. Finally, a compact T-type power divider is used for connecting the two signal paths. As can be seen in Figure 1(c), the network provides four output ports (ports 2, 3, 4, and 5). Ports 2 and 3, with equal amplitude and 90° phase shifts, are connected to the two short metal probes to feed the lower band radiation patch, while ports 4 and 5 are connected to the two long metal probes to feed the upper band radiation patch. Thus, two orthogonal

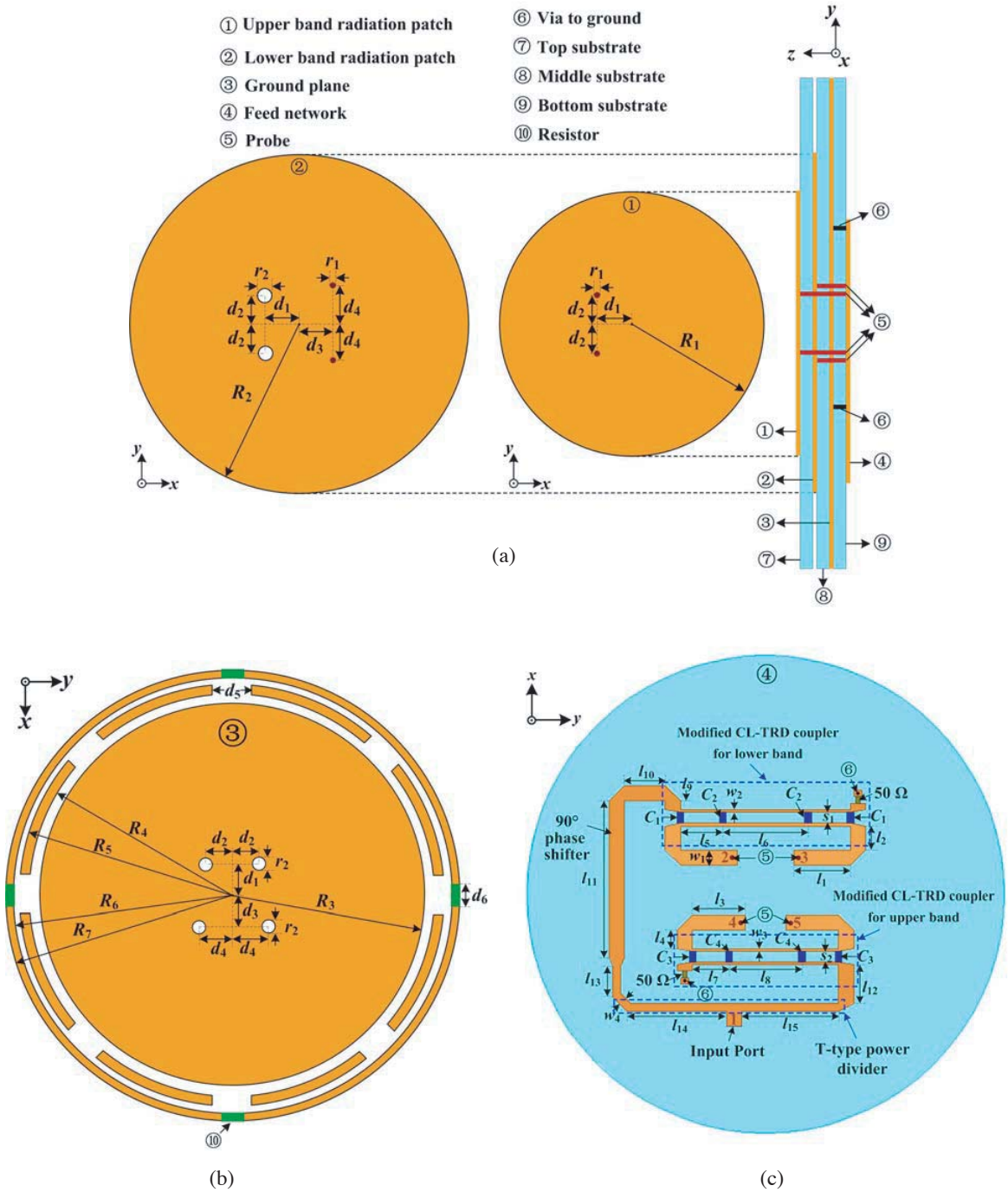


**Figure 1.** Geometry of the proposed dual-band CPMA. (a) Radiation patches. (b) AMSL-GP. (c) Feed network.

modes on the two patches are excited, resulting in dual-band CP radiation waves. The input port (port 1) is connected to coaxial cables. The modeling and simulation of the proposed dual-band CPMA are performed with 3-D full-wave EM simulation software HFSS. Main dimensions of the antenna are listed in Table 1.

**Table 1.** Dimensions of the proposed dual-band antenna with wide 3-dB ARBW (unit: mm, pF).

| $R_1$ | $R_2$ | $R_3$ | $R_4$ | $R_5$ | $R_6$ | $R_7$ | $w_1$ | $w_2$ | $w_3$ |
|---|---|---|---|---|---|---|---|---|---|
| 31.8 | 40.75 | 53 | 55 | 57 | 58 | 59 | 3.76 | 0.72 | 0.72 |
| $d_1$ | $d_2$ | $d_3$ | $d_4$ | $d_5$ | $d_6$ | $r_1$ | $r_2$ | $s_1$ | $s_2$ |
| 7 | 7 | 9 | 9 | 10 | 6 | 0.9 | 3 | 2.4 | 2.4 |
| $l_1$ | $l_2$ | $l_3$ | $l_4$ | $l_5$ | $l_6$ | $l_7$ | $l_8$ | $l_9$ | $l_{10}$ |
| 14 | 5.87 | 13 | 4.5 | 10.5 | 21 | 9 | 18 | 2.09 | 10 |
| $l_{11}$ | $l_{12}$ | $l_{13}$ | $l_{14}$ | $l_{15}$ | $C_1$ | $C_2$ | $C_3$ | $C_4$ | $R_L$ |
| 38.72 | 9.5 | 7.8 | 24.6 | 23.8 | 1.5 | 2.5 | 1.0 | 1.8 | 20 Ω |

## 3. DESIGN PROCEDURE AND PARAMETRIC STUDY

### 3.1. Design Procedure of the Proposed AMSL-GP with Resistors

In this section, the contributions of the AMSL-GP and edge resistors to the antenna's 3-dB ARBW are investigated. Figure 2 shows design evolutions of the proposed AMSL-GP. The evolution starts from GP-I, which is composed of only a circular ground patch (without AMS). Based on the analysis in [24], it is found that the 3-dB ARBW has its maximum value when the ground diameter is around $0.6\lambda$. Thus, the size of the GP-I is chosen as $0.6\lambda$ (corresponding to 1.207 GHz).

To improve the 3-dB ARBW of the antenna, AMSs are inserted to the circular ground patch, as shown by GP-II. It is composed of a circular ground patch, an inner AMS, and an outer AMS. The AMSs are served as parasitic radiators on the ground, which will affect the ARBW of the main radiation. Here, the inner and outer AMSs are both divided into 4 sections by identical air gaps. To further enhance the 3-dB ARBW, edge resistors are inserted to replace the gaps at the outer AMS, as

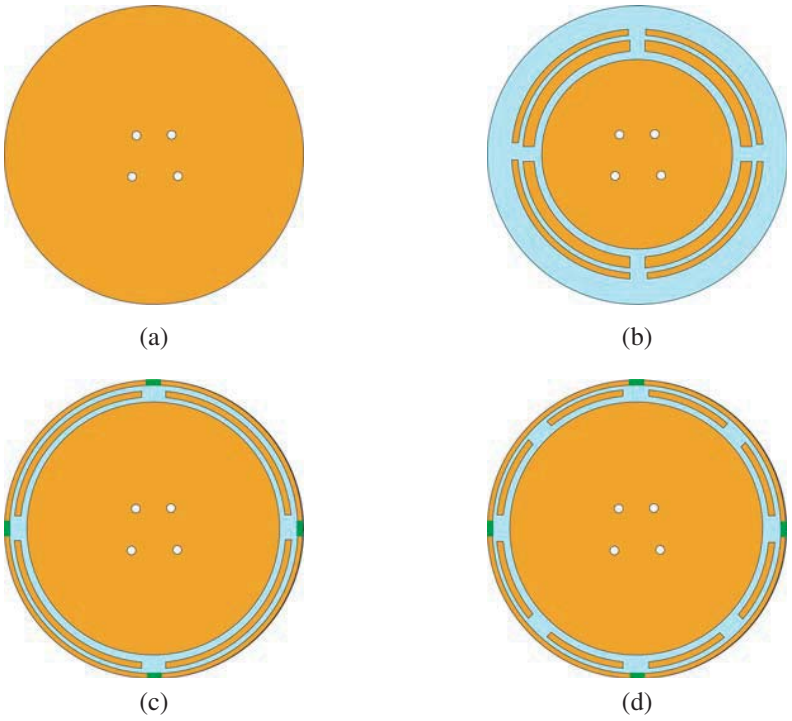


**Figure 2.** The design evolutions of the AMSL-GP. (a) GP-I. (b) GP-II. (c) GP-III. (d) GP-IV.

shown by GP-III. The resistors are in series with the outer AMS, and the outer AMS is located at the edge of the bottom substrate. Due to the edge resistor, the scattered wave transmitted to the edges can be absorbed, and the ARBW is enhanced. Since the resistors on the inner AMS have small influence on the ARBW of the antenna, this state is not given. By simply dividing the inner AMS of GP-III into 8 sections, the structure of GP-IV is shaped. It is noted that during the evolution, the dimensions of the substrate, as well as the sizes of the radiation patches, are fixed. Simulations are done using the stacked patches combined with the four GPs. The feature of the feed network is not considered. Moreover, the simulated results used for comparison are the optimal performances, including good impedance match (VSWR $< 2$), better AR at $\theta = 0°$ (AR $< 1$ dB), and widest 3-dB ARBW.

ARBWs of the antenna in the $xoz$ plane at 1.207 and 1.561 GHz are simulated with different GPs. The obtained results are presented in Figure 3. Table 2 illustrates the simulated 3-dB ARBWs. Obviously, when no AMS is added, corresponding to GP-I, the 3-dB ARBWs at the two center frequencies are the narrowest (176°/1.207 GHz and 182°/1.561 GHz). When using GP-II, 3-dB ARBWs of the antenna are both widened, which means that the insertion of AMSs contributes to the enhancement of the 3-dB ARBW. Comparing GP-III with GP-II, it is found that the 3-dB ARBW at the lower band is enhanced, while the value at upper band is nearly unchanged. It indicates that the 3-dB ARBW at the lower band can be improved by the edge resistors. In the evolution, resistors are also added to the inner AMS, and ARBWs of the antenna at 1.207 and 1.561 GHz are simulated. It is found from the results that the effects of the inner resistor are less than that of the outer resistors, which can be ignored. Thus, this case is not provided in the paper. Based on GP-III, a modified structure is presented (GP-IV) by simply dividing the inner AMS into 8 sections. It is observed from Table 2 that the 3-dB ARBW at upper band is obviously broadened using GP-IV, and the 3-dB ARBW at lower band is slightly improved. Finally, the antenna with GP-IV can produce the widest ARBWs both at the lower and upper center frequencies (203°/1.207 GHz and 215°/1.561 GHz).

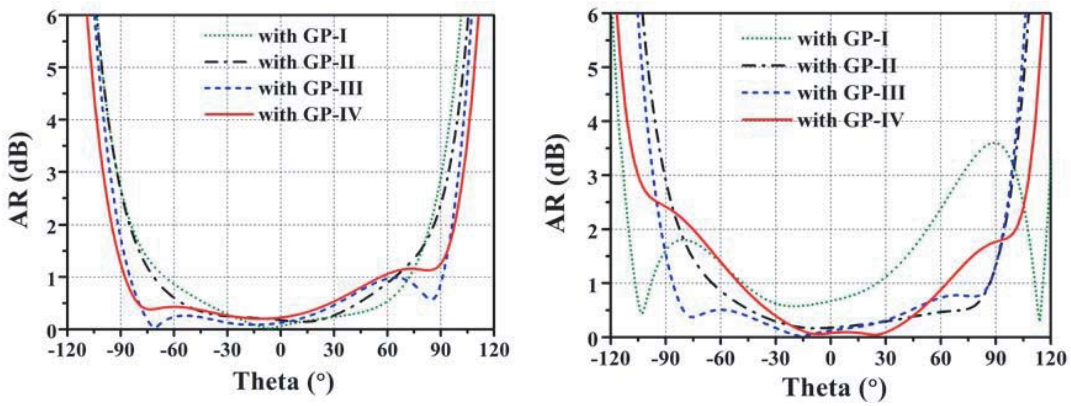


**Figure 3.** Simulated ARBWs for different GPs. (a) 1.207 GHz. (b) 1.561 GHz.

**Table 2.** 3-dB ARBWs of the antennas with different GPs.

| Frequency (GHz) | | 1.207 | 1.561 |
|---|---|---|---|
| 3-dB ARBW | GP-I | 176° | 182° |
| | GP-II | 187° | 191° |
| | GP-III | 196° | 195° |
| | GP-IV | 203° | 215° |

### 3.2. Parametric Study and Discussion

In order to investigate the effects of the AMS and the resistors, a parametric study is carried out using HFSS. Figure 4(a) shows the effect of the width of the AMS on the antenna 3-dB ARBW. It reveals that as the width of inner AMS ($R_5 - R_4$) increases from 0.5 to 2.0 mm, the 3-dB ARBWs at the two center frequencies are increased, while when the width ($R_5 - R_4$) increases from 2.0 to 3.5 mm, the 3-dB ARBWs are decreased. Thus, the optimal value of ($R_5 - R_4$) is 2.0 mm. When the width of the outer AMS ($R_7 - R_6$) is set to 0.75 mm, peak 3-dB ARBW at 1.207 GHz is obtained, while the widest 3-dB ARBW for 1.561 GHz is reached when the width is 1 mm. Since the change of 3-dB ARBW at 1.207 GHz is more stable than that at 1.561 GHz, the value of ($R_7 - R_6$) is chosen as 1 mm.

Figure 4(b) shows the effect of the gap of the AMS on the antenna 3-dB ARBW. It is observed that as the gap of inner AMS ($d_5$) increases from 4 to 10 mm, the 3-dB ARBWs at the two center frequencies are increased. On the other hand, when the width ($d_5$) increases from 10 to 16 mm, the 3-dB ARBWs are decreased. Moreover, the 3-dB ARBWs at 1.561 GHz are more strongly affected by the inner AMS gap than at 1.207 GHz. Since the edge resistors are in series with the outer AMS, the dimensions of the outer AMS gap ($d_6$) are chosen according to the lengths of several commercial resistors. It is revealed that the 3-dB ARBWs of the antenna at the two center frequencies are increased when the gap ($d_6$) varies from 2 mm to 6 mm. Figure 5 shows the simulated 3-dB ARBWs in the $xoz$ plane at 1.207 and 1.561 GHz for different values of resistors. It is observed that when the values of the resistors increase from 5 to 30 Ω, the 3-dB ARBW at 1.207 GHz is increased, while the 3-dB ARBW at 1.561 GHz is almost decreased. A peak 3-dB ARBW is obtained at 1.561 GHz when the value of the resistor is 20 Ω.

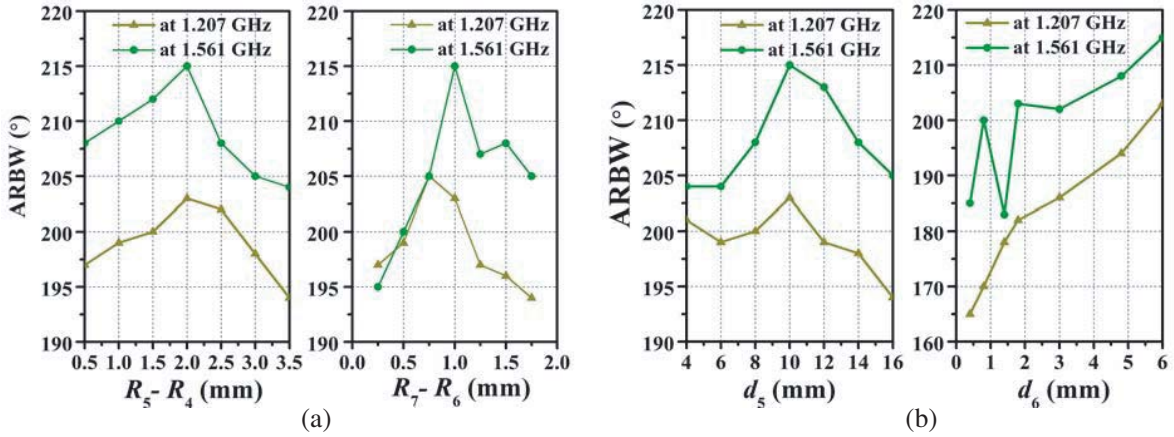


**Figure 4.** Effect of the AMS on the antenna 3-dB ARBW. (a) Effect of width. (b) Effect of gap.

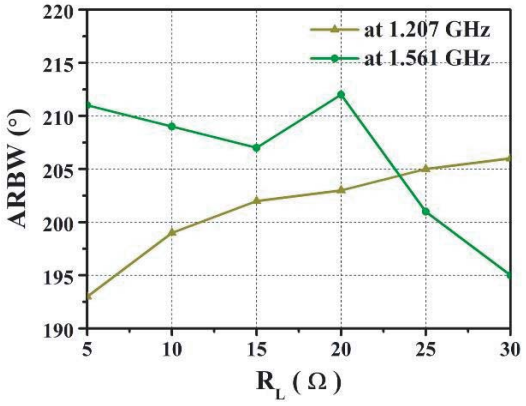


**Figure 5.** Simulated 3-dB ARBWs for different resistors.

### 3.3. Design of the Feed Network

Figure 6 shows the simulated results of the designed feed network. It is observed that the bandwidth equals 62.6% from 1.0 to 1.912 GHz for 10-dB return loss. Under the criterion of ($|S_{21}|$, $|S_{31}|$, $|S_{41}|$, $|S_{51}|$) = −6.0 dB ±0.5 dB, the bandwidths for the lower and upper bands are 4.8% and 16%, respectively. The phase differences between output ports for the two bands ($\angle S_{21} - \angle S_{31}$, $\angle S_{41} - \angle S_{51}$) are 90°± 5° over the bandwidths of 36.3% and 52.6%, respectively. The results demonstrate that the designed feed network provides consistent 90° phase shift on the equal output signals.

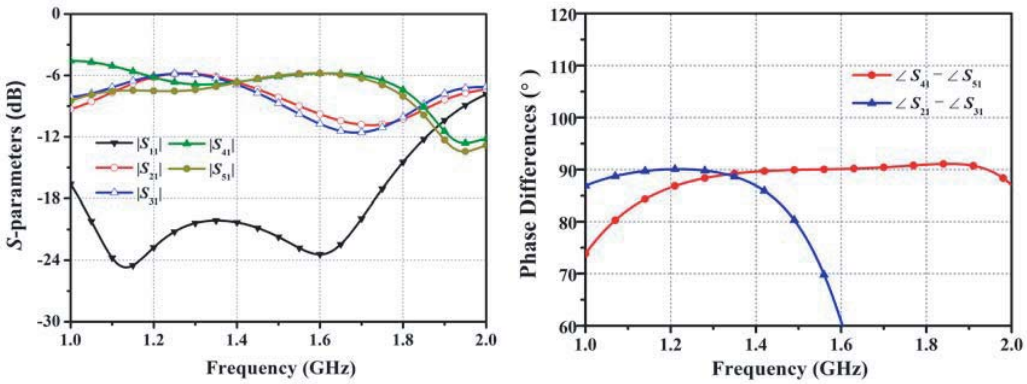


**Figure 6.** Simulated results of the designed single-input feed network. (a) $S$-parameters. (b) Output ports phase difference.

## 4. IMPLEMENTATION AND MEASURED RESULTS

To validate the proposed method, a prototype is designed, fabricated, and measured. Figure 7 shows photographs of the prototype. The overall size is 118 mm × 118 mm × 4.5 mm. $|S_{11}|$ of the fabricated antenna is measured by an Agilent N5230A vector network analyzer. The far-field feature is measured in an anechoic chamber. Figure 8 shows the simulated and measured $|S_{11}|$, gain, and AR of the antenna. For $|S_{11}| < -10$ dB, the measured bandwidth is from 1.15 to 1.65 GHz. For AR < 3 dB, the measured bandwidths are 9.6% (1.18 ∼ 1.3 GHz) for the lower band and 7.1% (1.48 ∼ 1.59 GHz) for the upper band, which can over the operating bandwidths of BDS, GPS L1/L2, and GLONASS L2. In the two bands, the proposed antenna exhibits measured peak gains of 1.98 dBic at 1.21 GHz and 4.1 dBic at 1.57 GHz. The measured AR is different from the simulated results, which is mainly caused by the errors coming from the fabrication, installation, and riding position in the anechoic chamber.

Figure 9 shows the simulated and measured radiation patterns of the antenna in the *xoz* and *yoz* planes at 1.207 and 1.561 GHz. The measured front-to-back ratios are more than 15 and 18 dB in the lower and upper frequencies, respectively. The measured half power beamwidths (HPBW) are about 91° and 85° at 1.207 and 1.561 GHz, separately. The measured and simulated ARs at 1.207 and 1.561 GHz in the *xoz* and *yoz* planes are plotted in Figure 10. The simulated ARBWs at 1.207 GHz are 198° and 185° in *xoz* and *yoz* planes, while the measured values are 185° and 187°. The simulated ARBWs at 1.561 GHz are 222° and 199° in *xoz* and *yoz* planes, while the measured values are 192° and 194°. The measured ARBWs are narrower than the simulated ones, which is mainly due to the errors in installation. In general, the proposed antenna can achieve the 3-dB ARBW of at least 185° at the two frequencies.

Table 3 compares our design with some previous dual-band CP antennas. Firstly, the size of the proposed antenna is the smallest. In impedance bandwidth, AR bandwidth, and ARBW, the proposed antenna shows better performance than the antennas in [15, 18, 19]. Although the antenna in [17] exhibits wider bandwidth than the proposed structure, the 3-dB ARBW is narrow. In [20], cross dipoles and cavity have to be used. The design complexity and cost are increased by the proposed structure. In applications, microstrip antennas are more preferred due to their low profile, light weight,

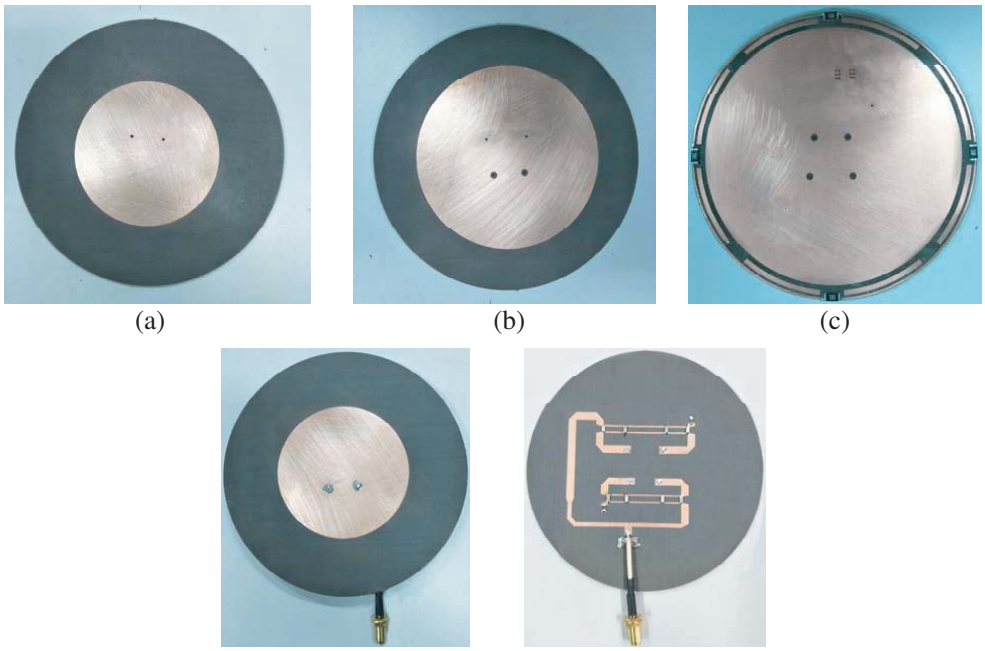

**Figure 7.** Photograph of the fabricated prototype. (a) Upper band radiation patch. (b) Lower band radiation patch. (c) GP. (d) Top and bottom view of the integrated antenna.

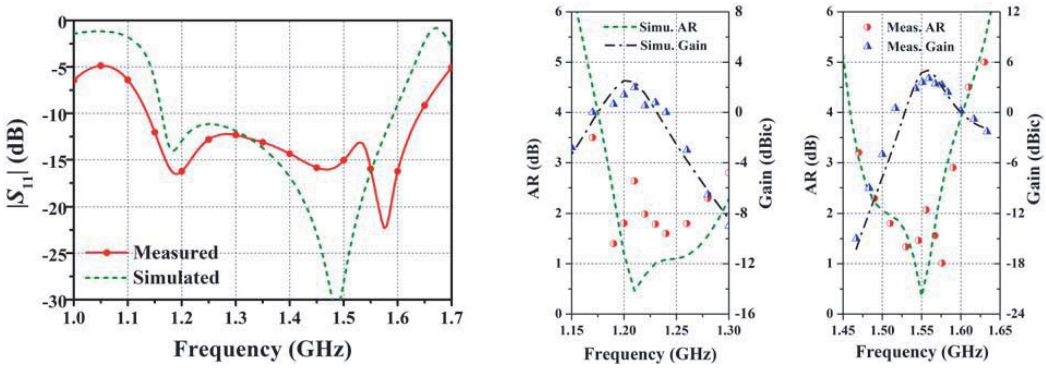


**Figure 8.** Measured and simulated performance of the fabricated antenna. (a) $|S_{11}|$. (b) Gain and AR.

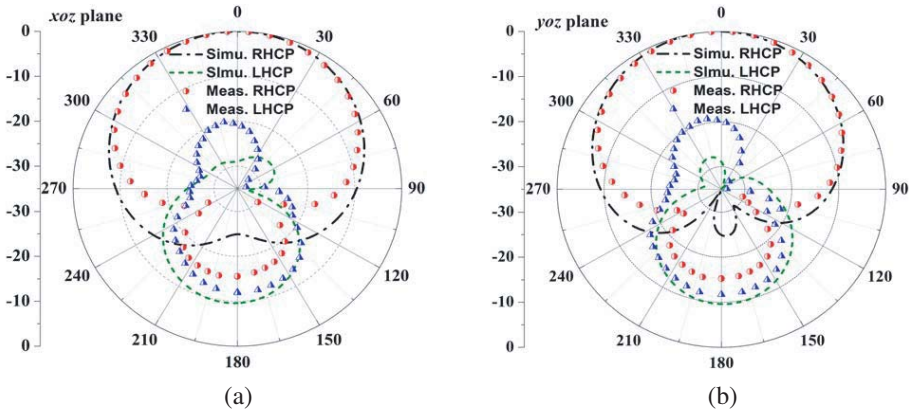

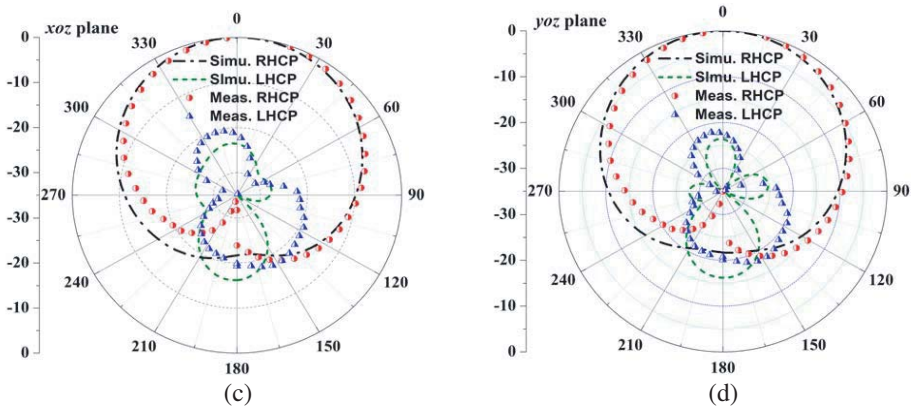


**Figure 9.** Measured and simulated radiation pattern in *xoz* and *yoz* planes. (a) 1.207 GHz. (b) 1.561 GHz.

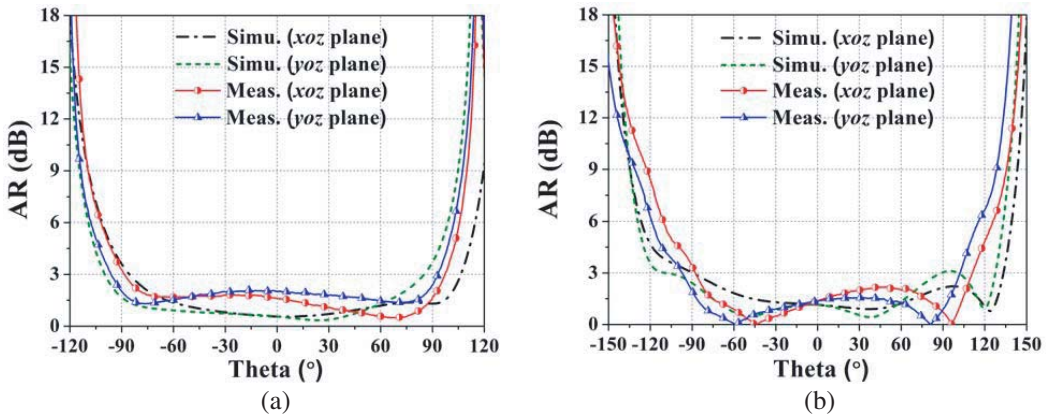


**Figure 10.** Measured and simulated AR as a function of elevation angle in *xoz* and *yoz* planes. (a) 1.207 GHz. (b) 1.561 GHz.

**Table 3.** Comparison between our design and some previous dual-band CP antennas.

| Ref. | Method | Overall size ($\lambda_0{}^a$) | Freq. (GHz) | 10-dB bandwidth | 3-dB AR bandwidth | Gain (dBic) | HPBW$^b$ | 3-dB ARBW$^b$ |
|---|---|---|---|---|---|---|---|---|
| [16] | Meandered-line shaped ring patch | 0.448×0.448×0.077 | 1.615 | 2.3% | 0.6% | 4.3 | – | $> 85°$ |
| | | | 2.491 | 7.2% | 1.4% | 6.38 | – | $> 85°$ |
| [18] | Patch with broadband four-feed circuit | 0.7×0.8×0.09 | 1.4 | 75.8 % | 75.8% | 3 ∼ 6 | $< 60°$ | 74° |
| | | | 1.8 | | | | | 54° |
| | | | 2.2 | | | | | 45° |
| [19] | Stacked patch with extended substrate | 0.484×0.484 | 1.451 | 2.3% | 0.62% | 3.9 | 100° | 165° |
| | | | 2.029 | 3.1% | 0.69% | 3.9 | 114° | 175° |
| [20] | Crossed dipole cavity | 0.491×0.491×0.164 | 1.227 | 6.3% | 1.87% | 6.3 | – | 132° |
| | | | 1.575 | 22.0% | 6.7% | 7.5 | – | 143° |
| [21] | Single vertical cross Dipole with cavity | 0.573×0.573×0.296 | 1.227 | 46.3% | 13.0% | 4.39 | 103° | 202° |
| | | | 1.575 | | 30.2% | 5.06 | 111° | 211° |
| **This work** | **Patch antenna with AMSL-GP** | **0.475×0.475×0.03** | **1.207** | **35.7%** | **9.6%** | **1.98** | **91°** | **185°** |
| | | | **1.561** | | **7.1%** | **4.1** | **85°** | **192°** |

and compact structure. Compared with the CPMA in [15, 17, 18], it is demonstrated that the proposed AMSL-GP can enhance the 3-dB ARBW of stacked patch antennas obviously.

## 5. CONCLUSION

In this study, a dual-band CPMA with wide 3-dB ARBW is designed and fabricated. Wide 3-dB ARBW of more than 185° at the two bands is achieved with the proposed AMSL-GP. Moreover, with the employment of the CL-TRD coupler based feed network, wide impedance and AR bandwidths are obtained. The measured results indicate that the proposed CPMA is suitable for dual-band BDS applications to improve system angular coverage.

## ACKNOWLEDGMENT

This work was supported in part by the National Natural Science Foundation of China (Nos. 51809030, 61571075 and 61871417), in part by the China Post-Doctoral Science Foundation (No. 2017M611210), in part by the Doctor Startup Foundation of Liaoning Province (No. 20170520150), and in part by the Fundamental Research Funds for the Central Universities (Nos. 3132019211 and 3132019219).

## REFERENCES

1. Zeng, D. Z. and Q. X. Chu, "Cavity-backed self-phased circularly polarized multidipole antenna with wide axial-ratio beamwidth," *IEEE Antennas Wireless Propag. Lett.*, Vol. 16, 1998–2001, 2017.
2. Wang, S. Y., X. Zhang, L. Zhu, and W. Wu, "Single-fed wide-beamwidth circularly polarized patch antenna using dual-function 3-D printed substrate," *IEEE Antennas Wireless Propag. Lett.*, Vol. 17, No. 4, 649–653, Apr. 2018.
3. Luo, Y., Q. X. Chu, and L. Zhu, "A low-profile wide-beamwidth circularly-polarized antenna via two pairs of parallel dipoles in a square contour," *IEEE Trans. Antennas Propag.*, Vol. 63, No. 3, 931–936, Mar. 2015.
4. Bai, X., J. Tang, X. Liang, J. Geng, and R. Jin, "Compact design of triple band circularly polarized quadrifilar helix antennas," *IEEE Antennas Wireless Propag. Lett.*, Vol. 13, 380–383, 2014.
5. Yang, Y.-H., J.-L. Guo, B.-H. Sun, and Y.-H. Huang, "Dual-band slot helix antenna for global positioning satellite applications," *IEEE Trans. Antennas Propag.*, Vol. 64, No. 12, 5146–5152, Dec. 2016.
6. Choi, E. C., J. W. Lee, and T. K. Lee, "Modified S-band satellite antenna with isoflux pattern and circularly polarized wide beamwidth," *IEEE Antennas Wireless Propag. Lett.*, Vol. 12, 1319–1322, 2013.
7. Tang, C. L., J. Y. Chiou, and K. L. Wong, "Beamwidth enhancement of a circularly polarized microstrip antenna mounted on a three-dimensional ground structure," *Microw. Opt. Technol. Lett.*, Vol. 32, No. 2, 149–153, Jan. 2002.
8. Su, C. W., S. K. Huang, and C. H. Lee, "CP microstrip antenna with wide beamwidth for GPS band application," *Electron. Lett.*, Vol. 43, No. 20, 1062–1063, Sep. 2007.
9. Bao, X. L. and M. J. Ammann, "A cavity-backed spiral slot antenna with wide axial ratio beamwidth for GPS system," *Microw. Opt. Technol. Lett.*, Vol. 56, No. 5, 1050–1054, May 2014.
10. Son, H. W., H. Park, K. H. Lee, G. J. Jin, and M. K. Oh, "UHF RFID reader antenna with a wide beamwidth and high return loss," *IEEE Trans. Antennas Propag.*, Vol. 60, No. 10, 4928–4932, Oct. 2012.
11. Wang, M. S., X. Q. Zhu, Y. X. Guo, and W. Wu, "Compact circularly polarized patch antenna with wide axial-ratio beamwidth," *IEEE Antennas Wireless Propag. Lett.*, Vol. 17, 714–718, Apr. 2018.
12. Liu, N. W., L. Zhu, and W. W. Choi, "Low-profile wide-beamwidth circularly-polarised patch antenna on a suspended substrate," *IET Microw. Antennas Propag.*, Vol. 10, No. 8, 885–890, May 2016.

13. Zhang, X., L. Zhu, and N. W. Liu, "Pin-loaded circularly-polarized patch antennas with wide 3-dB axial ratio beamwidth," *IEEE Trans. Antennas Propag.*, Vol. 65, No. 2, 521–528, Feb. 2017.
14. Zhang, X., L. Zhu, N. W. Liu, and D. P. Xie, "Pin-loaded circularly-polarized patch antenna with sharpened gain roll-off rate and widened 3-dB axial ratio beamwidth," *IET Microw. Antennas Propag.*, Vol. 12, No. 8, 1247–1254, 2018.
15. Sun, C., H. L. Zheng, and Y. Liu, "Compact dual-band circularly polarized GNSS antenna," *Electron. Lett.*, Vol. 51, No. 20, 1559–1560, Oct. 2015.
16. Chen, K., J. D. Yuan, and X. Y. Luo, "Compact dual-band dual circularly polarized annular-ring patch antenna for BeiDou navigation satellite system application," *IET Microw. Antennas Propag.*, Vol. 11, No. 8, 1079–1085, May 2017.
17. Zhang, Y. Q., X. Li, L. Yang, and S. X. Gong, "Dual-band circularly polarized annular-ring microstrip antenna for GNSS applications," *IEEE Antennas Wireless Propag. Lett.*, Vol. 12, 615–618, May 2013.
18. Liu, Q., Y. Li, Z. G. Mo, and Y. A. Liu, "Compact broadband circularly-polarised directional universal GNSS antenna with symmetric radiation pattern and stable near zenith coverage," *IET Microw. Antennas Propag.*, Vol. 11, No. 5, 657–663, 2017.
19. Bao, X. L. and M. J. Ammann, "Dual-frequency dual circularly-polarised patch antenna with wide beamwidth," *Electron. Lett.*, Vol. 44, No. 21, 1233–1234, Oct. 2008.
20. Ta, S. X., I. Park, and R. W. Ziolkowski, "Dual-band wide-beam crossed asymmetric dipole antenna for GPS applications," *Electron. Lett.*, Vol. 48, No. 25, 1580–1581, Dec. 2012.
21. Sun, Y. X., K. W. Leung, and J. Ren, "Dual-band circularly polarized antenna with wide axial ratio beamwidths for upper hemispherical coverage," *IEEE Access*, Vol. 6, 58132–58138, Oct. 2018.
22. Shie, C. I., J. C. Cheng, S. C. Chou, and Y. C. Chiang, "Trans-directional coupled-line couplers implemented by periodical shunt capacitors," *IEEE Trans. Microw. Theory Techn.*, Vol. 57, No. 12, 2981–2988, Dec. 2009.
23. Liu, H., S. Fang, Z. Wang, and T. Shao, "Coupled line trans-directional coupler with improved power distribution and phase performance," *2017 IEEE International Symposium on Radio-Frequency Integration Technology (RFIT)*, 126–128, Seoul, 2017.
24. Rezazadeh, N. and L. Shafai, "Study of finite ground plane effects in circularly polarized circular microstrip antennas," *2016 17th International Symposium on Antenna Technology and Applied Electromagnetics (ANTEM)*, 2016, DOI: 10.1109/ANTEM.2016.7550228.